



Comprehensive Stability Design of Steel Members and Systems via Inelastic Buckling Analysis – Beam-Column Validation Studies

Oğuzhan Toğay¹ and Donald W. White²

Abstract

This paper provides an overview of a comprehensive approach for the design of structural steel members and systems via an Inelastic Nonlinear Buckling Analysis (INBA) that includes appropriate column, beam and beam-column inelastic stiffness reduction factors. The stiffness reduction factors are derived from the ANSI/AISC 360 Specification column, beam and beam-column strength provisions. The resulting procedure provides a relatively rigorous check of member design resistances accounting for continuity effects across braced points, as well as lateral and/or rotational restraint from other framing including a wide range of types and configurations of stability bracing. With this approach, no separate checking of the corresponding Specification member stability design resistance equations is required. The buckling analysis captures these resistances. In addition, no calculation of effective length (K) factors and moment gradient and/or load height (C_b) factors, is necessary. The buckling analysis directly captures the fundamental mechanical responses associated with these design strength factors. This approach is coupled with the AISC Direct Analysis Method (the DM), for calculation of the pre-buckling displacement effects, to fully satisfy the stability design requirements of the AISC Specification. In addition to explaining the method's key concepts, the paper focuses on validation of the method for capture of the lateral-torsional buckling response of general doubly-symmetric I-section beam-columns subjected to major-axis bending. Results from the recommended approach and from routine application of the DM are compared to the results from test simulation per Appendix 1.3 of the AISC Specification.

1. Introduction

Engineers are accustomed to the use of effective length (K) and stiffness reduction (τ) factors to assess the strength of members in the context of the AISC Effective Length Method (the ELM). With the ELM, the structure is modeled predominantly as a geometrically perfect, nominally elastic system. The only consideration of geometric imperfections in the analysis is for gravity-only load combinations ($\Delta_o = 0.002L$). The Direct Analysis Method (DM) improves upon the ELM by including the effects of geometric imperfections and reductions in stiffness in the second-order structural analysis to determine the load effects. Because of its accuracy in capturing the stability

¹ Graduate Research Assistant, Georgia Institute of Technology, <oguzhantogay@gatech.edu>

² Professor, Georgia Institute of Technology, <don.white@gatech.edu>

limit states, the DM may be applied all types of structures. Conversely, the AISC Specification disallows the usage of the ELM for stability critical structures having substantial sidesway amplification. In addition, with the DM, the calculation of K factors is not necessary. All members considered in this method are taken as braced (usually with $K = 1$) in the resistance calculations.

This paper presents a procedure that combines the qualities of the DM for the calculation of the overall load effects with the qualities of an inelastic nonlinear buckling analysis (INBA) to assess general prismatic or non-prismatic member resistances including influence of the bracing and member end restraints. The INBA method uses all the same requirements for the load-deflection analysis as in the DM, but replaces the traditional equation-based evaluation of member buckling based resistances by an equivalent inelastic buckling analysis solution. If the INBA procedure is conducted for a full structure, or a subassembly of a full structure, it can directly account for interactions between adjacent members and between the members and their bracing systems, in the determination of the component strengths, including the characteristics of the restraint provided to inelastic members from other less yielded members and from elastic bracing. In addition, the INBA approach allows for simpler modelling of structures that are loaded predominantly in one plane, since a three-dimensional analysis considering out-of-plane imperfections is not required.

This paper first gives an overview of the Inelastic Nonlinear Buckling Analysis (INBA) approach. Then, an overview of test simulation studies used to evaluate the INBA and the routine DM is provided. Following a discussion of the various methods that are employed, the parameters of the study are presented. Finally, an analysis of the data from this study is discussed.

2. Methodology

2.1 Proposed Inelastic Nonlinear Buckling Analysis Approach

Inelastic Nonlinear Buckling Analysis (INBA) generally is a buckling analysis that considers both material nonlinearity and pre-buckling displacements. For general beam-column members, pre-buckling displacements commonly have a measurable influence on the structural capacity. As such, the AISC Specification generally requires the use of a second-order load-deflection analysis to determine the load effects. The specific INBA approach proposed by the authors involves the use of a DM solution for the pre-buckling load-deflection analysis, but replaces the member stability based resistance equations of the Specification by equivalent inelastic buckling analysis solutions. The inelastic buckling analysis utilizes stiffness reduction factors that many engineers are accustomed to for members subjected to concentric axial loading. However, it also uses stiffness reduction factors associated with the Specification lateral torsional buckling equations to allow for the evaluation of beam LTB responses. The recommended INBA solution uses a basic interpolation between the column and beam inelastic stiffness reduction factors to address general beam-column member stability limit states. This approach employs a Thin-Walled Open-Section (TWOS) frame element for the buckling calculations. This element has seven degrees of freedom at each joint or nodal location – three translations, three rotations, and one warping degree of freedom, which allows for the important consideration of member warping rigidity in the evaluation of member stability limit states involving torsion. The INBA solutions presented in this paper are conducted using the SABRE2 software (White et al. 2016).

2.1.1. Recommended Updates to the AISC/AASHTO Flexural Resistance Equations

Prior to discussing the details of the INBA procedures, it is essential to discuss an important change that is needed to the AISC/AASHTO flexural resistance equations to allow for accurate capture of experimental test and advanced test simulation results by the refined inelastic buckling analysis procedures.

Subramanian et al. (2016) propose that, in light of additional experimental and advanced test simulation data generated since the original calibration of the unified provisions, as well as the availability of simple estimates of inelastic LTB effective length factors and the emergence of practical capabilities that accurately account for inelastic end restraint effects, several modifications of the unified, AISC and AASHTO resistance equations should be considered:

1. The value of L_p should be taken as $0.63r_t\sqrt{E/F_y}$.
2. The nominal compression flange stress, at which yielding and geometric imperfection effects start to impact the LTB resistance, should be reduced to F_{yr} (AASHTO) and F_L (AISC) = $0.5F_{yc}$.
3. The noncompact web slenderness limit (λ_{rw}) should be set as

$$\lambda_{rw} = \max\left(5.7\sqrt{\frac{E}{F_{yc}}}, \min\left((3.1 + 2.5\frac{A_{fc}}{A_{wc}})\sqrt{\frac{E}{F_{yc}}}, 4.6\sqrt{\frac{E}{F_{yc}}}\right)\right) \quad (1)$$

Subramanian et al. (2016) show that these changes result in a more uniform level of reliability, as a function of the LTB slenderness, consistent with the minimum target of $\beta = 2.6$ for statically determinate beams intended in the AISC LRFD Specification (2016).

In Figure 1, an example beam-column plot for DS-1, a W21x44 rolled section with 144 in unbraced length, is provided. This figure shows an example calculation of the results from:

- Refined test simulations based on Appendix 1.3 of the AISC (2016) Specification using one-half of typical nominal residual stresses and geometric imperfections, denoted by the term Appendix 1.3*.
- Direct Analysis Method solutions using Inelastic Nonlinear Buckling Analysis based on the AISC (2016) resistance equations modified as discussed above, denoted by the term INBA*.
- Routine DM solutions using the AISC (2016) Specification provisions with the above flexural resistance changes recommended by Subramanian et al. (2016), denoted by the term DM*.
- Refined test simulations per AISC (2016) using full typical nominal residual stresses and geometric imperfections, denoted by the term Appendix 1.3, and
- Routine Direct Analysis Method solutions using the current AISC (2016) flexural resistance equations, denoted by the term DM.

The nominal residual stresses for rolled I section members and the nominal geometric imperfections considered in this work are discussed in Sections 2.2.3 and 2.2.4. Subramanian and White (2016) show that reduced nominal residual stresses and geometric imperfections are

necessary for advanced test simulation results to provide a close correlation with experimental test data for I type of cross-sections.

Subsequently, the Appendix 1.3* solution is employed as the benchmark finite element simulation in this work. As can be observed from Fig. 1, without modifying the AISC flexural resistance equations, the moment capacity is predicted too optimistically. When the results from the Appendix 1.3 solutions (using full nominal residual stresses and geometric imperfections) are compared to the DM solutions based on the current Specification flexural resistance equations, the over-prediction by the DM solutions is substantial.

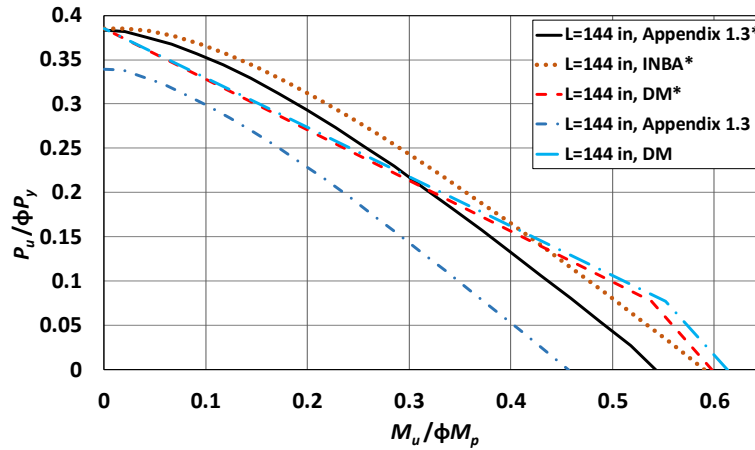


Figure 1: DS-1 (W21x44) L=144 in, Uniform Primary Moment Current versus Recommended

2.1.2 Column Inelastic Stiffness Reduction Factor τ_a

The column inelastic stiffness reduction factor (τ_a) is derived from AISC Specification column equation. This derivation is presented in detail by White et al. (2016).

If inelastic column buckling controls the overall behavior, $\left(\frac{\Gamma P_u}{\phi_c P_{ye}} > 0.390 \right)$

$$\tau_a = -2.724 \frac{\Gamma P_u}{\phi_c P_{ye}} \ln \left(\frac{\Gamma P_u}{\phi_c P_{ye}} \right) \quad (2)$$

For $\left(\frac{\Gamma P_u}{\phi_c P_{ye}} \leq 0.390 \right)$, where elastic buckling controls the behavior,

$$\tau_a = 1 \quad (3)$$

where: P_u = Required axial strength

P_{ye} = Cross-section plastic axial strength ($P_{ye} = A_e F_y$)

Γ = Applied load ratio

ϕ_c = Resistance factor for compression

In the 2016 AISC Specification, slender cross-section elements under uniform axial compression are calculated with a unified effective width approach. Therefore, the member effective area (A_e) is used in the τ_a calculations instead of the gross area (A_g). This results in the following column net stiffness reduction factor (SRF)

$$SRF = 0.9 \times 0.877 \times \tau_a \frac{A_e}{A_g} \quad (4)$$

This stiffness reduction factor is applied to EI_x , EI_y , EC_w and GJ .

2.1.3 Beam Inelastic Stiffness Reduction Factor τ_{ltb}

The beam lateral torsional buckling stiffness reduction factor, τ_{ltb} , is derived in a manner similar to τ_a . The following discussion summarizes the corresponding equations in a concise generalized form. Regardless of the I-section member type, if the member satisfies $m \leq \frac{R_b F_L}{F_{yc}}$,

$$\tau_{ltb} = 1 \quad (5)$$

where $m = \frac{\Gamma M_u}{\phi_b M_{yc}}$, M_u is the required flexural strength, M_{yc} represents the moment at yielding of the extreme fiber in the compression flange, and ϕ_b is the resistance factor for flexure. The term R_b is the web bend buckling strength reduction factor, equal to 1.0 for a compact and noncompact web sections and less than 1.0 for slender web sections.

If a compact or noncompact web member satisfies $\frac{F_L}{F_{yc}} < m < \frac{\phi_b M_{max.LTB}}{\phi_b M_{yc}}$,

$$\tau_{ltb} = \frac{\sqrt{Y^4 X^2}}{\sqrt{6.76 X^2 \left(\frac{F_{yc}}{E}\right)^2 m^2 + 2Y^2}} \quad (6)$$

whereas, if a slender web member satisfies $\frac{R_b F_L}{F_{yc}} < m < \frac{\phi_b M_{max}}{\phi_b M_{yc}}$,

$$\tau_{ltb} = \frac{m}{R_b} \left[\frac{\left(R_h - \frac{m}{R_b}\right)}{\left(R_h - \frac{F_L}{F_{yc}}\right)} \left(\sqrt{\frac{F_{yc}}{F_L}} - \frac{1.1}{\pi} \right) + \frac{1.1}{\pi} \right]^2 \quad (7)$$

The corresponding generalized net inelastic stiffness reduction factor is

$$SRF = 0.9 R_b \tau_{ltb} \quad (8)$$

This net stiffness reduction factor is applied to EI_y , EC_w and GJ .

In the above limits on the usage of Eqs. 6 and 7,

$$\phi_b M_{max.LTB} = 0.9 R_b R_{pc} M_{yc} \quad (9)$$

This expression is the generalized ‘‘plateau strength’’ of the LTB curve, equal to $0.9M_p$ if the cross-section has a compact web, where M_p is the section plastic moment. In addition, the term R_{pc} is equal to R_h for hybrid slender web sections, where R_h is the hybrid cross-section factor defined in AASHTO (2015). In this case, Eq. 9 becomes $0.9R_b R_h M_{yc}$.

Furthermore, in Eq. 6,

$$Y = m \left[\frac{\left(1 - \frac{m}{R_{pc}}\right)}{\left(1 - \frac{F_L}{R_{pc} F_{yc}}\right)} \left(\frac{L_r}{r_t} - \frac{L_p}{r_t} \right) + \frac{L_p}{r_t} \right] \left(\frac{F_{yc}}{E} \right) \left(\frac{1}{1.95} \right) \quad (10)$$

and

$$X^2 = \frac{S_{xc} h_o}{J} \quad (11)$$

Lastly, the term $m = \frac{\Gamma M_u}{\phi_b M_{yc}}$ can be written generally as

$$m = R_b R_{pc} \frac{\Gamma M_u}{\phi_b M_{max}} \frac{\phi_b M_{max}}{\phi_b M_{max.LTB}} \quad (12)$$

where

$$\phi_b M_{max} = \min(\phi_b M_{max.LTB}, \phi_b M_{n.FLB}, \phi_b M_{n.TFY}) \quad (13)$$

is the maximum possible flexural resistance considering all the applicable limit states of lateral torsional buckling, flange local buckling, and tension flange yielding. The terms $\phi_b M_{n.FLB}$ and $\phi_b M_{n.TFY}$ are the flange local buckling and tension flange yielding design resistances. The term $\phi_b M_{n.LTB}$ is referred to by the AISC Specification as the compression flange yielding resistance.

2.1.4 Beam-Column Stiffness Reduction Factor

When the member is under both axial and flexural loading, the τ_a and τ_{ltb} equations are calculated using the unity check (UC) values instead of the $\Gamma P_u / \phi_c P_{ye}$ and $\Gamma M_u / \phi_b M_{max}$ ratios. White et al. (2016) shows a close correlation between the corresponding INBA predicted strengths and I-section beam-column resistances. In addition, it is recommended that the UC equations in the INBA solutions should be based on the cross-section type:

1. When the section has slender plates under axial compression, or noncompact or slender plates under flexural compression,

$$UC = \Gamma P_u / \phi_c P_{ye} + \Gamma M_u / \phi_b M_{max} \quad (14a)$$

2. Otherwise, the UC equations are taken from the AISC 2016 Specifications as

$$UC = \Gamma P_u / \phi_c P_{ye} + 8/9 \Gamma M_u / \phi_b M_{max} \quad \text{for } \Gamma P_u / \phi_c P_{ye} \geq 0.2 \quad (14b)$$

$$UC = \Gamma P_u / 2\phi_c P_{ye} + \Gamma M_u / \phi_b M_{max} \quad \text{for } \Gamma P_u / \phi_c P_{ye} < 0.2 \quad (14c)$$

Given the above equations the beam-column *SRF* is interpolated between the corresponding column and beam values using the following equation:

$$SRF = \left(\frac{\zeta}{90^\circ} \right) 0.9 \times 0.877 \times \tau_a \frac{A_e}{A_g} + \left(1 - \frac{\zeta}{90^\circ} \right) 0.9 R_b \tau_{ltb} \quad (15)$$

where ζ , is calculated as

$$\zeta = a \tan \left(\frac{P_u / \phi_c P_{ye}}{M_u / \phi_b M_{max}} \right) \quad (16)$$

The above beam-column stiffness reduction factor is applied to EC_w , EI_y and GJ .

2.2 Design Assessment by Test Simulation

In this paper, test simulation solutions based on AISC (2016) Appendix 1.3, using reduced residual stresses and geometric imperfections from commonly employed values, are employed as the “gold standard” for evaluation of the results from the recommended DM solutions using INBA as well as the solutions from routine DM solutions. As stated previously, this type of test simulation solution, is denoted by Appendix 1.3*. In addition, the terms INBA* and DM* highlight the fact that these solutions are based on modified AISC 2016 flexural resistance equations per Subramanian et al. (2016). In the following subsections, the attributes of the AISC Appendix 1.3* calculations employed in this study are detailed.

2.2.1 Finite Element Model

The ABAQUS 6.14 (Simulia 2014) finite element analysis software is employed to model the members considered in these study. In all cases, a full nonlinear shell finite element solutions using the S4R element is used to model for both webs and flanges. The S4R is a four node quadrilateral large strain shell element formulation. The mesh is generated with 12 elements for the width of

the flanges, and 20 elements for the web depth. The shell element aspect ratio is chosen approximately 1.0 in the web to calculate the number of the elements along the member lengths.

2.2.2 Material Properties

Homogenous material properties are used for all the members with the yield stress (F_y) of 50 ksi, and the modulus of the elasticity (E) of 29,000 ksi. The material properties F_y and E are multiplied by 0.9, as required by AISC 2016 Appendix 1.3. The factored properties are denoted by F_y^* and E^* . For the yield plateau of the material, the tangent stiffness is modeled as $E/1000$ up to ten times the yield strain (ϵ_y). After this point, the strain hardening modulus is taken as $E/50$. At the levels of the strains that are observed in the test simulations, true stress versus log strain and engineering stress versus engineering strain are essentially the same.

2.2.3 Residual Stresses

Residual stress patterns of one-half the commonly-assumed Lehigh pattern (Galambos and Ketter 1959) for rolled sections and the Best-fit Prawel (Kim (2010)) pattern for welded sections are provided in Figs. 2 and 3. These residual stresses are recommended by Subramanian and White (2016) as appropriate values necessary for close correlation with lateral torsional buckling experimental test results.

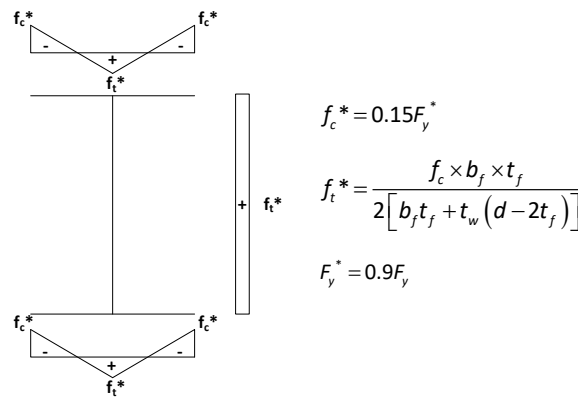


Figure 2: One-Half of Lehigh Residual Stress Pattern, for Rolled I-Sections

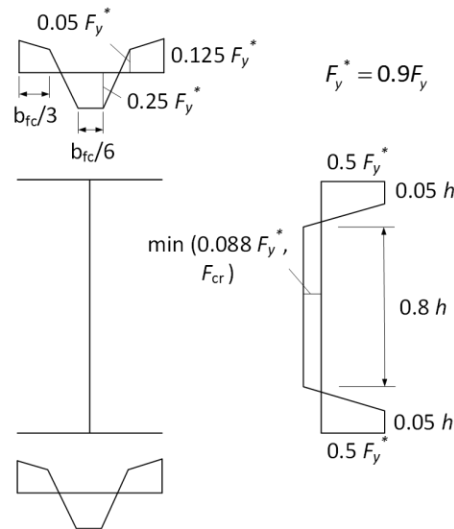


Figure 3: One-Half of Best-Fit Prawel Residual Stress Pattern, for Welded I-Sections

2.2.4 Geometric Imperfections

The test simulations are based on out-of-straightness patterns with one-half of the AWS (2010)/AISC Code of Standard Practice (COSP) (2016) geometric imperfection tolerance values unless noted otherwise. Subramanian and White (2016) show that these reduced geometric imperfections are necessary for close correlation with experimental results.

Flange tilt and web out-of-flatness patterns are obtained by elastic eigenvalue buckling analysis of the members with the out-of-plane displacements restrained at the top and bottom flange-web juncture points, and with the members being subjected to uniform axial compression. Given the resulting buckling modes, the flange tilt and web-out-flatness are isolated and scaled to one-half the tolerance values as illustrated in Fig. 4.

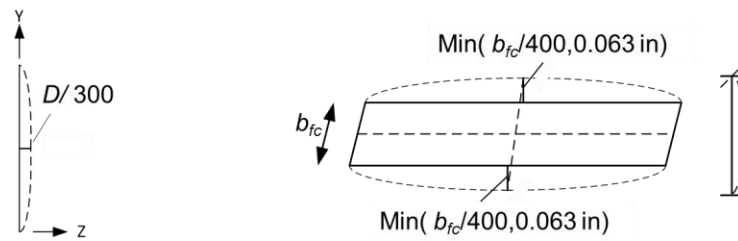


Figure 4: Web Out-of-Flatness and Flange Tilt Imperfection

The resulting flange tilt and web out-of-flatness imperfections are combined with a flange sweep that is applied at web-flange juncture points. If the flange under consideration is subjected to flexural compression, a sinusoidal flange sweep is applied to the flange in flexural compression. For a flange that is in flexural tension, zero sweep ($IF = 0$) is applied if the net force in the flange is tension (Fig. 5). Otherwise a flange sweep between zero to $L_b/2000$ is applied as a linear function of IF . This handling of the sweep in flexural tension is illustrated by the IF factor shown in Fig. 6.

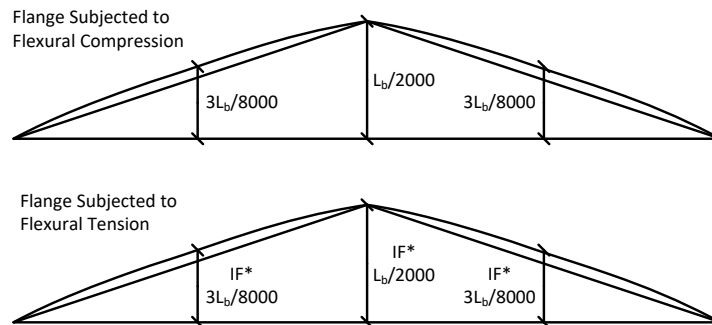


Figure 5: Applied Imperfections (One-Half of the AWS/AISC COSP Flange Sweep Tolerance)

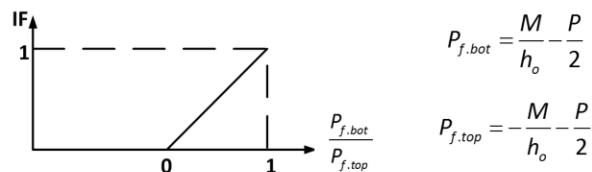


Figure 6: IF (Tension Flange Sweep Scale Factor) Calculation

3. Beam-Column Validation Studies

As noted in the introduction, this paper assesses the accuracy of two Direct Analysis Method solutions. One is referred to routine Direct Analysis Method and uses the AISC stability based resistance equations, and the other is an explicit inelastic buckling analysis to determine buckling based resistances. The proposed Inelastic Nonlinear Buckling Analysis (INBA*) procedure as well as the routine DM procedure are evaluated for prediction of the lateral torsional buckling resistance of a wide range of doubly-symmetric I-section members.

In the following presentations, a post-fix “*” is appended to the names INBA and DM to emphasize that these calculations are all based on modified AISC flexural resistance equations recommended by Subramanian et al. (2016). In addition, the post fix “*” is also appended to Appendix 1.3, to emphasize that the test simulation solutions are based on one-half the residual stresses and geometric imperfections.

3.1. Load Configurations and Cross-Sections

Three different loading configurations are examined in this work. First, uniform primary moment cases with nine prismatic cross-sections are tested (Fig. 7). Second, moment gradient cases using the same prismatic cross-section set are evaluated (Fig. 8). Lastly, various W21x44 beam-columns subjected to uniformly distributed lateral load are studied (Fig. 9). A total of $609 + 588 + 63 = 1260$ test simulations are conducted.



Figure 7: Uniform Primary Moment Load Configuration



Figure 8: Moment Gradient Load Configuration

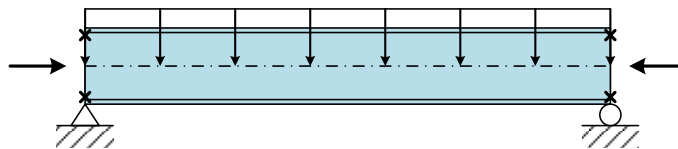


Figure 9: Uniformly Distributed Lateral Load Configuration

All the members are flexurally and torsionally simply-supported at their ends and they have no intermediate lateral bracing. As such, their effective lengths $L_{cx} = L_{cy} = L_{cz}$ are all equal to their laterally unbraced length L . Subramanian et al. (2016) and Togay et al. (2016) compare the results of INBA solutions to a relatively comprehensive database of I-section flexural tests involving various loading and end restraint conditions. Nine different cross-sections are considered in this study as summarized by Table 1. Members with short, intermediate and long unbraced lengths are considered for each of these sections.

Table 1: Doubly-Symmetric I-sections considered in validation studies ($b_f = 6.5$ in, $d_w = 19.8$ in).

Case	Description	t_f (in)	t_w (in)	$A_{fillats}$ (in ²)	$b_f/2t_f$	d_w/t_w
1	W21x44 Section	0.4500	0.3500	0.22	7.22	56.57
2	Equivalent Welded Section	0.4500	0.3500	0.00	7.22	56.57
3	Noncompact Web	0.4500	0.1787	0.00	7.22	110.80
4	Slender Web	0.4500	0.1238	0.00	7.22	160.00
5	Noncompact Flange	0.2708	0.3500	0.00	12.00	56.57
6	Noncompact Flange & Noncompact Web	0.2708	0.1787	0.00	12.00	110.80
7	Noncompact Flange & Slender Web	0.2708	0.1238	0.00	12.00	160.00
8	Slender Flange & Noncompact Web	0.1806	0.1787	0.00	18.00	110.80
9	Slender Flange & Slender Web	0.1806	0.1238	0.00	18.00	160.00

3.2. Example Results

Beam-column interaction plots that compare the INBA* and DM* results with the Appendix 1.3* solutions are provided in Toğay and White (2016). The plots are provided for all the cases for the uniform primary and the moment gradient loading conditions shown in Table 1. For the uniformly distributed loading, only the DS-1 (W21x44 rolled section) is studied. To illustrate a typical beam-column interaction plot, the DS-2 uniform primary moment case with $L = 144$ in (DS-2-UM-L144) length is selected (Fig. 10).

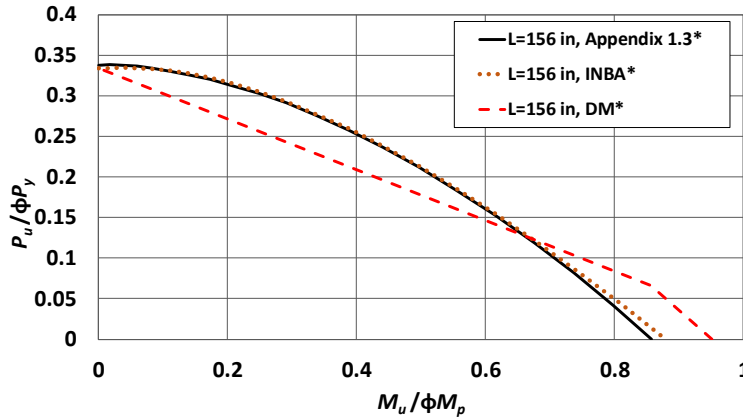


Figure 10: Example Beam-Column Interaction Plot (DS-2 Moment Gradient Loading with 156 in Unbraced Length)

3.3 Error Calculation Procedure

For evaluation of each method, a normalized beam-column plot is used. In this plot, the normalization is performed using the Appendix 1.3* maximum axial strength ($P_{sim,max}$) and maximum flexural strength ($M_{sim,max}$) values (Fig. 11).

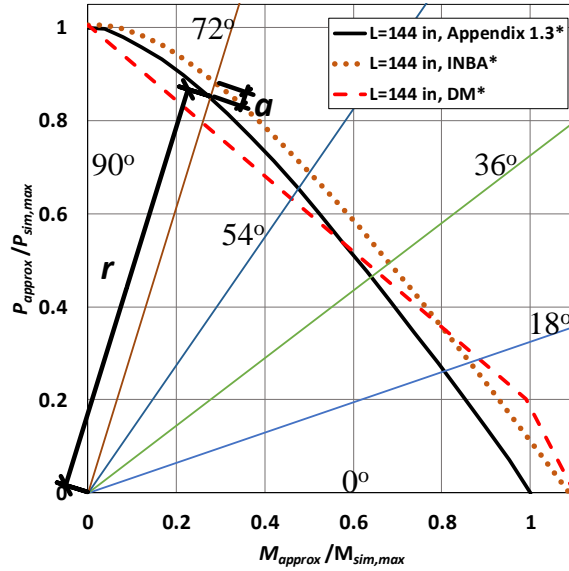


Figure 11: Normalized Beam-Column Interaction Plot (Example Case: DS-1 L = 144 in Uniform Moment Loading)

Using five equally spaced radial lines on the normalized interaction plot, the percentage errors in the DM* and INBA* solutions, relative to the Appendix 1.3* solutions, are calculated as

$$error(\%) = \left(\frac{a}{r} \right) \times 100 \quad (17)$$

where r is the distance from origin to the Appendix 1.3* result, and a is the distance between either Appendix 1.3* and INBA* results or Appendix 1.3* and DM* results.

The 0° line corresponds to the flexural (beam) loading case, while the 90° line corresponds to the pure axial compression case. The error plots are generated with the error values from Eq. 17 for each of the cross-section cases and load combinations. These plots are provided in Toğay and White (2016). An example error plot for DS-3 with 144 in unbraced length and uniform moment loading is provided in Fig. 12.

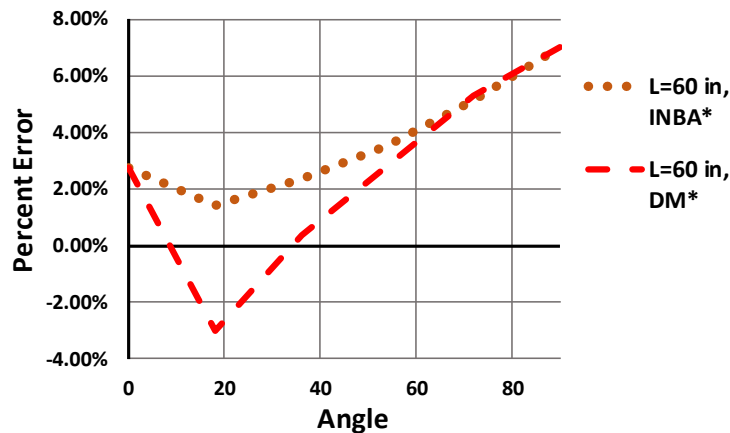


Figure 12: Error Plot (Example Case: DS-3 L = 60 in Uniform Moment Loading)

In Figs. 13 and 16, and Table 2, the corresponding errors for uniform primary moment, moment gradient and uniformly distributed load are provided, respectively.

4. Data Analysis

The uniform primary moment and moment gradient load combinations are studied for all the cross-section types listed in Table 1. For the uniformly distributed load combination, only the DS-1 cases with three different lengths are considered. The members are examined using Appendix 1.3* (test simulation studies), INBA* (the DM combined with inelastic nonlinear buckling analysis using Specification based stiffness reduction factors), and DM* (the AISC (2016) DM provisions). The recommended flexural resistance modifications from Subramanian and White (2016) are employed with the INBA and DM solutions, and the recommended modifications to typical residual stresses and geometric imperfections by these authors are employed with the Appendix 1.3 solutions, as denoted by the “*” symbol shown with the names. In the following subsections, Figs. 13 and 16 are provided to show the statistical analysis of the percent error along each of the radial lines presented in Fig. 10. The percent error values of each method are calculated with respect to the Appendix 1.3* test simulation results.

In Figs. 13 and 16, box and whiskers style format statistical analysis plots are provided for the uniform primary moment and moment gradient cases. In these plots, the black “x” inside the boxes represents the mean of each data set. The bottom and top of the light grey and dark grey boxes represent the first (Q_1) and third (Q_3) quartile points, respectively. The bottom whisker end point is calculated as $Q_1 - 1.5 \times IQR$, while the top whisker end point is at $Q_3 + 1.5 \times IQR$. In these equations, IQR is the interquartile range, calculated as $Q_3 - Q_1$. In addition, the solid horizontal lines inside the boxes represent the median value of the data sets. Outlier data points, defined as data points outside the whiskers, are presented as dots in the plots.

4.1 Uniform primary moment load combinations

In this section, the results for members with cross-sections listed in Table 1 are presented for the uniform primary moment (UM) load combinations (Fig. 7). The statistical results for the percent errors are provided by the box and whiskers plot in Fig. 13.

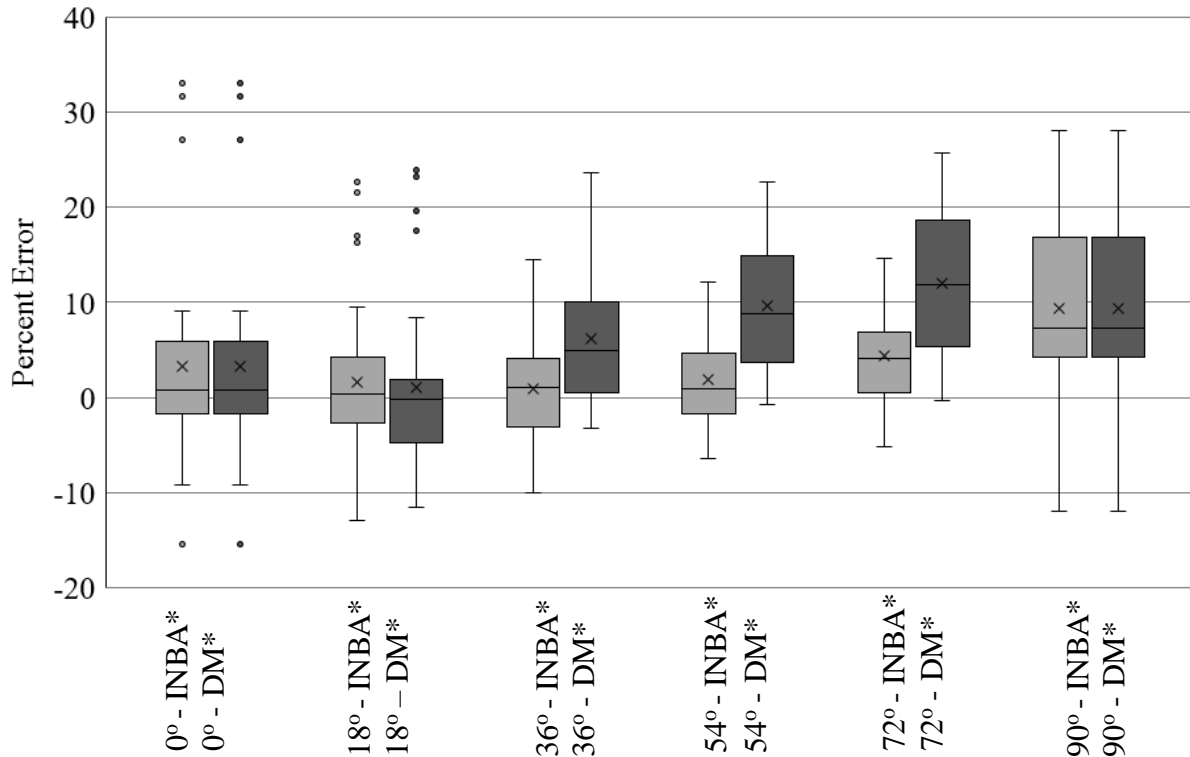


Figure 13: Comparison of INBA* and ELM/DM* versus Appendix 1.3 solutions for Uniform Primary Moment Load Configuration

The main finding from Fig. 13 is that, for all the axial compression and moment combinations, the average and median of the data sets are greater than zero, which corresponds to the conservative prediction for these cases. For 0° (uniform primary moment only) and 90° (axial compression only) cases, the INBA* solutions and DM* solutions match exactly with one another. The derivation of the column and beam stiffness reduction factors of the INBA* procedure ensures this.

The LTB strengths of DS-8 and DS-9, cross-sections with slender elements (Table 1), are defined as outliers in Fig. 13 for the 0° and 18° data sets. This is caused by the flange local buckling (FLB) limit states equations of the AISC Specification, which are captured by the INBA* or DM* solutions, being significantly conservative. An example case for DS-8 with 60 in unbraced length is provided in Fig. 14. The conservatism of the AISC FLB equations for these cases is due to the lack of consideration of the corresponding physical post-local buckling of the compression flange.

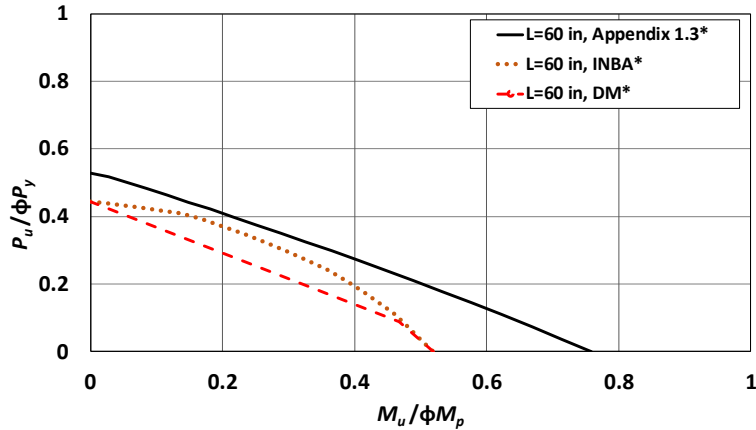


Figure 14: Example Slender Section Case with Uniform Primary Load Configuration (DS-8)

In addition, the maximum unconservative error in this data set is measured as 9%. The one unconservative outlier case, DS-1 with 24 in. length, is at 15.49% (Fig. 15). Although, one might expect the equivalent welded section (DS-2) provides lesser capacity than the rolled section (DS-1), it is observed that the capacity of the DS-1 is smaller than DS-2 for that particular length. This smaller capacity is mainly caused by the residual stress effects that are used in the test simulations. With the patterns that are used, the Lehigh residual stress pattern is actually more critical. The reason for this behavior is that the Lehigh pattern is based on light column-type sections where the web tends to be entirely in residual tension. With that type of residual stress distribution, the section has a net residual compression force in the flanges, which tends to be relatively damming. In addition, it can be argued that the Lehigh residual stress pattern is not representative of beam type wide flange sections. Subramanian and White (2016) show other more representative patterns, including a summary of past research measurements, but recommended the use of the Lehigh pattern with the reduced magnitude residual stresses as a single nominal pattern that can be applied for all rolled wide-flange shapes.

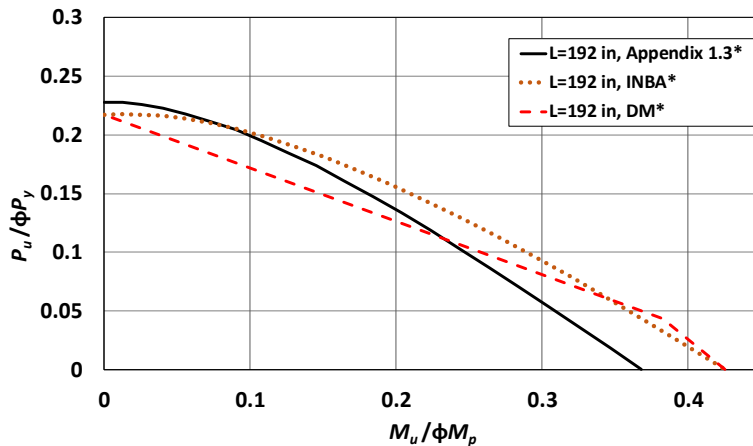


Figure 15: DS-1 L=24 in, Uniform Primary Moment Beam-Column Interaction Curve

For 90° cases, with only axial compression, the percent error values show a large variation. This is mainly caused by the use of only one column curve in the AISC provisions. Using more than one column curve would require more than one τ_a equation, but it would improve the results for both columns and beam-column.

The point having a significant change in slope in the beam-column interaction plots is referred as “knee point”. For the 18° case, which corresponds to the “knee” region, the INBA* solution shows closer correlation than DM*. The INBA* linear interaction equation for UC values helps to reduce unconservative errors in beam-column resistances (Fig. 10).

The intermediate angles (36°, 54°, 72°) of the beam-column interaction curves show that, INBA* provides closer correlation with the Appendix 1.3* solutions.

4.2 Moment Gradient Tests

In this section, the cross-sections in Table 1 are tested for moment gradient (MG) load combinations (Fig. 8). The statistical results of percent error values are provided by the box and whiskers plot in Fig. 16.

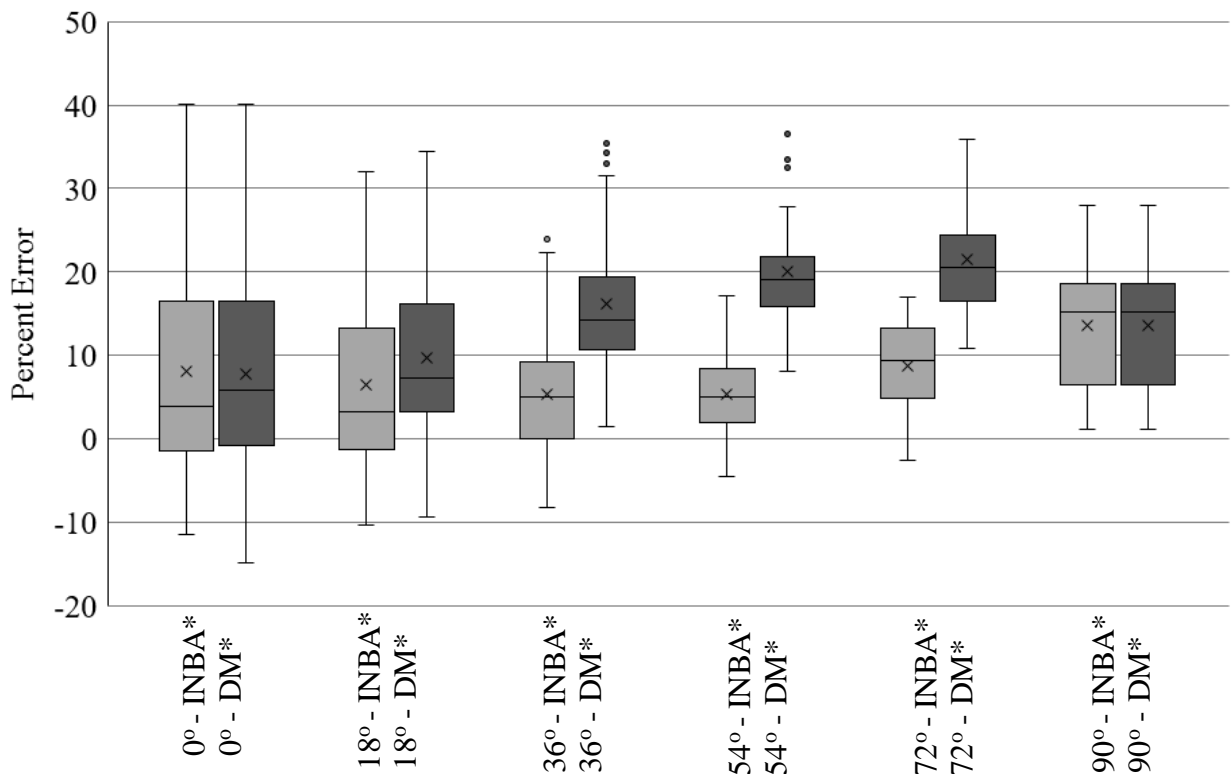


Figure 16: Comparison of INBA* and DM* versus Appendix 1.3 solutions for Moment Gradient Load Configuration

For all data sets in moment gradient load configurations, the mean and average values of the INBA* solutions show a closer match with the Appendix 1.3* results than the DM* solutions. The intermediate angles (18°, 36°, 54°, 72°) of the beam-column interaction curves show similar behavior to the corresponding uniform primary moment results. The average and mean values of the INBA* solutions are closer to zero than the DM* solutions for all the beam-column cases.

The INBA* and the DM* solutions are slightly different for the flexure only case on the moment gradient loading conditions (0° line on Fig. 11). The moment gradient factor of C_b is the main reason for this difference. The C_b that is employed in the moment gradient case DM* solutions is

provided by Salvadori (1956). This equation is used in the DM* solutions since it gives a better lower-bound for the LTB resistance for these cases (1.75) than the AISC Eq. F1-1 value of 1.67. As it can be observed from Fig. 1, the INBA* solutions provide better correlation with Appendix 1.3* solutions. This is because the INBA* solutions work directly with the inelastic *SRF* values along the member lengths.

The extreme conservative results for 0° cases is from the slender sections (DS-8 and DS-9). Figure 16 shows that influence of the FLB limit states on the resistance of the cross-section, as an example. The outliers are observed for the DM solutions in the data sets of 36° and 54°. One of the outlier cases is presented in Fig. 17.

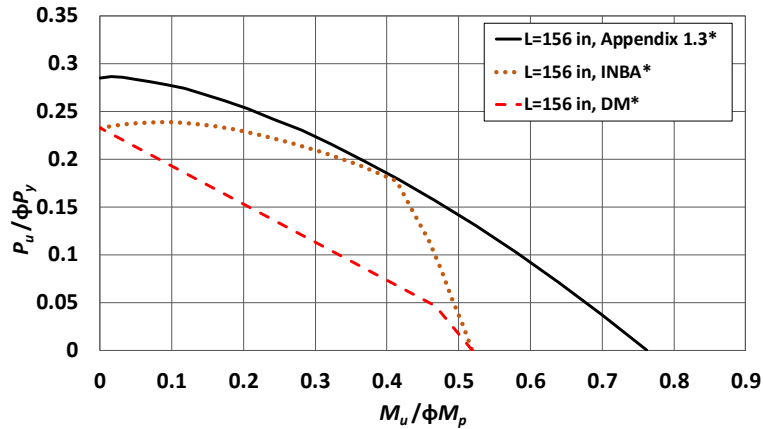


Figure 17: Example Slender Section Case with Moment Gradient Load Configuration (DS-8)

If the accuracy of the FLB provisions were to be improved, the use of Eqs. H1-1 (Eqs. 14b and 14c) is still conservative relative to the Appendix 1.3* results. The INBA* results give better correlation with this change (Fig. 18).

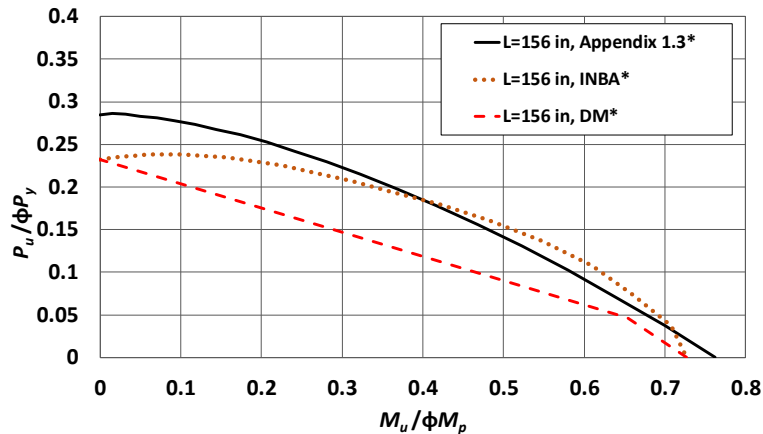


Figure 18: DS-8 L=144in, Moment Gradient Loading with Modified FLB strength

3.3 Uniformly Distributed Lateral Load Configuration

In this section, DS-1 (W21x44) is examined for uniformly distributed lateral load combinations with uniform axial compressions (Fig. 8). The error values related to this loading configurations are listed in Table 2. The findings for uniform primary moment load cases and moment gradient

loads are consistent with the uniformly distributed lateral load cases. For the smallest member length of 90 in, the INBA* results shows very close correlation with the Appendix 1.3* results.

As in the moment gradient load studies, there is a difference between INBA* and DM* solutions for pure flexure cases. This difference is mainly caused by the moment gradient factor of C_b . The C_b equations that is used for the moment gradient load configuration is not suitable to use in the uniformly distributed loading case since its moment diagram is not linear. The C_b equation used in these cases is obtain with the AISC Eq. F1-1 developed by Kirby and Nethercot (1979). Table 2 shows that using the INBA* approach provides a better correlation with the Appendix 1.3* solutions.

Table 2: DS-1 Uniformly Distributed Loads (W21x44 rolled section) Percent Error Values

Line Angle(°)	L= 90 in		L = 156 in		L = 204 in	
	INBA*	Chapter C*	INBA*	Chapter C*	INBA*	Chapter C*
0	-6.59	-11.40	-14.27	-16.12	-15.74	-15.12
18	-4.37	-11.61	-12.15	-13.00	-11.92	-9.91
36	-2.74	-3.48	-9.92	-2.66	-8.64	1.08
54	-1.22	2.60	-7.24	4.60	-4.73	8.78
72	3.18	7.33	-4.13	8.44	0.08	12.91
90	6.95	6.95	1.63	1.63	5.82	5.82

4. Conclusions

This paper evaluates the ability of routine Direct Analysis (DM) solutions, and an advanced form of the DM that uses Inelastic Nonlinear Buckling Analysis (INBA) to predict the strength of a large number of doubly symmetric prismatic I-section member. The INBA procedures provides a more general and more rigorous handling of all types of bracing, end restraint and continuity effects.

A large number of simulation studies are conducted to show that inelastic nonlinear buckling analysis with stiffness reduction factors derived from the AISC Specification provisions provides a close correlation with test simulation studies. The combined use of recommended modifications to the AISC/AASHTO flexural equations by Subramanian and White (2016) and the use of reduced geometric imperfections and residual stresses in test simulation procedures produces a close correlation between the DM, INBA and test simulation solutions. Subramanian et al. (2016) show improved correlation of corresponding solutions with a large data set of experimental test results.

References

- AASHTO (2015). *AASHTO LRFD Bridge Design Specifications, 7th Edition*, American Association of State Highway and Transportation Officials, Washington, DC.
- AISC (2016). *Specifications for Structural Steel Buildings, ANSI/AISC 360-16*, American Institute of Steel Construction, Chicago, IL.
- AWS (2010). *Structural Welding Code—Steel, AWS D1.1: D1.1M, 22nd ed*, AWS Committee on Structural Welding.
- Y.D. Kim, Behavior and Design of Metal Building Frames Using General Prismatic and Web-Tapered Steel I-Section Members, in: *School of Civil and Environmental Engineering, Georgia Institute of Technology*, Atlanta, GA., 2010.
- Prawel, S. P., Morrell, M. L., and Lee, G. C. (1974). "Bending and Buckling Strength of Tapered Structural Members." *Welding Research Supplement*, 53, 75-84.
- Simulia (2014). *ABAQUS/Standard Version 6.14-2*, Simulia, Inc, Providence, RI.

- Subramanian, L. P., Jeong, W. Y., Yellepeddi, R., and White, D. W. (2016). "Assessment of I-Section Member LTB Experimental Tests Using Inelastic Buckling Analysis." *Structural Engineering, Mechanics and Materials Report No. 110*, School of Civil and Environmental Engineering, *Georgia Institute of Technology*, Atlanta, GA.
- Subramanian, L. P., and White, D. W. (2016). "Reassessment of the Lateral Torsional Buckling Resistance of I-Section Members – Uniform Moment Studies." *Submitted for Consideration by the Journal of Constructional Steel Research*.
- Toğay, O., and White, D. W. (2016). "Ultimate Strength Predictions for Doubly-Symmetric I-Section Beam-Columns using Test Simulation, Inelastic Nonlinear Buckling Analysis, Ordinary DM Calculations, and Advanced Elastic Analysis ", *Georgia Institute of Technology*, Atlanta, GA.
- Toğay, O., Jeong, W. Y., Subramanian, L. P., and White, D. W. (2016)., " Load Height Effects on Lateral Torsional Buckling of I-Section Members - Design Estimates, Inelastic Buckling Calculations and Experimental Results", *Georgia Institute of Technology*, Atlanta, GA.
- White, D. W., Jeong, W. Y., and Toğay, O. (2016). "Comprehensive Stability Design of Steel Members and Framing Systems via Inelastic Buckling Analysis (in press)." *International Journal of Steel Structures* 16(4): 1-14 (2016).
- White, D. W., Jeong, W. Y., and Toğay, O. (2016). "SABRE2." <white.ce.gatech.edu/sabre>(Dec 19,2016).
- T.V. Galambos, R.L. Ketter, Columns under combined bending and thrust, *Journal of the Engineering Mechanics Division*, ASCE 85 (1959) 135–152.
- Kirby, P.A. and Nethercot, D.A. (1979), Design for Structural Stability, *John Wiley & Sons, Inc.*, New York, NY.
- Salvadori, M. (1956), "Lateral Buckling of Eccentrically Loaded I-Columns," *Transactions of the ASCE*, Vol. 122, No. 1.